UNIVERSITAT DE BARCELONA

FACULTAT DE QUÍMICA

DEPARTAMENT DE QUÍMICA FÍSICA

Programa de Doctorat de Tecnologia de Materials

Bienni 2004-2006

Electrochemical preparation of Co-Ag nanostructured materials for GMR applications

Memòria que presenta JOSÉ MANUEL GARCÍA TORRES per optar al títol de Doctor per la Universitat de Barcelona

Directores de la tesi:

Dra. Elvira GÓMEZ VALENTÍN
Professora Titular de Química Física
Universitat de Barcelona

Dra. Elisa VALLÉS GIMÉNEZ
Professora Titular de Química Física
Universitat de Barcelona

CHAPTER 7

Co_{Core}-Ag_{Shell} NANOPARTICLES

7

Co_{Core}-Ag_{Shell} NANOPARTICLES

Finally, the preparation of magnetic/non-magnetic nanoparticles with giant magnetoresistance was also attempted. In section 7.1, the fabrication and characterization of Co-Ag nanoparticles with core-shell structure will be presented. After that, the magnetic and magnetotransport properties as well as the strategy developed to measure the later property will be dealt with in section 7.2.

7.1. Synthesis and characterization of Co@Ag core-shell nanoparticles

$Co_{Core}Ag_{Shell}$ nanoparticles were prepared by the water in oil (W/O) microemulsion method. A two step reduction process was followed to fabricate the core-shell structure. In a first step, cobalt nucleus was obtained which acted as a seed for the growth of the silver shell in a second stage. Whereas cobalt core size was constant, the thickness of the silver shell was modified by changing silver concentration in the microemulsion.

Nearly monodisperse nanoparticles were obtained, with mean sizes in the range 3-5 nm depending on the silver shell thickness. Firstly, TEM studies allowed observing the core-shell nature of the synthesized nanoparticles. However, it was the use of HRTEM together with fast fourier transform (FFT) that clearly revealed the $Co_{Core}Ag_{Shell}$ arrangement. XRD together with electron diffraction determined the hcp and fcc structure of cobalt and silver, respectively. No signs of solid solution were observed. Although cobalt core was metallic, cobalt oxides were detected by XPS, their content being higher for unprotected cobalt nanoparticles. The optical properties were also studied by recording the UV-Vis spectra. Surface plasmon (SP) resonance peak appeared after covering the cobalt core with silver. Moreover, a red shift on the SP peak of $Co_{Core}Ag_{Shell}$ nanoparticles was observed in comparison with pure silver nanoparticles. The electrochemical characterization of cobalt, silver and

Co-Ag nanoparticles was also performed. Important differences in the voltammetric response of the three kinds of nanoparticles were observed. These differences allowed using cyclic voltammetry as a tool to determine the correct core-shell formation.

GROUP OF ARTICLES INCLUDED IN SECTION 7.1.

Page 253: Synthesis and characterization of Co@Ag core-shell nanoparticles

Jose Garcia-Torres, Elisa Vallés and Elvira Gómez, Journal of Nanoparticle Research DOI 10.1007/s11051-009-9784-x

Synthesis and characterization of Co@Ag core-shell nanoparticles

J Nanopart Res
DOI 10.1007/s11051-009-9784-x

RESEARCH PAPER

Synthesis and characterization of Co@Ag core–shell nanoparticles

Jose Garcia-Torres · Elisa Vallés · Elvira Gómez

Received: 19 May 2009 / Accepted: 15 October 2009

Abstract A micellar method has been used to prepare silver-coated cobalt (Co@Ag) nanoparticles. The synthesized particles have been deeply characterized by several methods, i.e., XRD, UV–Vis, TEM, XPS, and electrochemical techniques. There is every indication that the obtained particles show a truly core–shell structure. All the nanoparticles obtained under different conditions are in the size range 3–5 nm. High-resolution TEM (HRTEM), Fast Fourier Transformation (FFT), and Selected Area Electron Diffraction (SAED) indicated that the presence of hcp-Co and fcc-Ag, in which cobalt is located in the central area; meanwhile silver is at the edges of the nanoparticle. The absorption band of the Co@Ag colloid shifts to a longer wavelength and broadens relative to that of pure silver colloid. Voltammetric characterization allowed to determine the coverage of the cobalt core.

Keywords Co@Ag nanoparticles · Microemulsion method · Structure · Optical properties · Cyclic voltammetry · Composite nanomaterials

J. Garcia-Torres · E. Vallés · E. Gómez (✉)
Electrodep., Departament de Química Física, Institut de Nanociència i Nanotecnologia (IN2UB) de la Universitat de Barcelona, Martí i Franquès, 1, 08028 Barcelona, Spain
e-mail: e.gomez@ub.edu

Introduction

The physical properties of nanoscale metal particles are presently the object of intensive research. The novel physical properties that these materials display is mainly attributed to surface or quantum size effects (Schmid 1994; Halperin 1986). The control of the nanocluster's properties will therefore be highly dependent upon the strict control of both the particle size and the chemical bonding at the surface. Moreover, the decrease in the particle size promotes higher reactivity, modifying superficial properties. Bimetallic nanocomposites having core–shell structure have received special attention because of their electronic, magnetic, optical and chemical, or biological properties (Hodak et al. 2000; Andres et al. 1996; Schmid 1998). Examples include magnetic resonance imaging for medical diagnosis, high-density magnetic recording, controlled drug delivery, catalysis, and energy conversion. Significant attention is paid on hybrid nanomaterials composed of magnetic and non-magnetic parts. Good examples of this type of materials are bimetallic nanoparticles like Fe@Au, Co@Ag, Co@Cu, etc., in which the non-reactive metallic coverage of the magnetic nanoparticles seems a suitable protecting tool.

A number of methods have been used to prepare the bimetallic nanoparticles including coprecipitation of the corresponding salts from solution (Tourinho et al. 1990), high-temperature decomposition of organic precursors (Hyeon et al. 2001), or

Published online: 30 October 2009

microemulsions (Solla-Gullón et al. 2003), among others. Water-in-oil (w/o) microemulsions are transparent, isotropic and thermodynamically stable with nano-sized water droplets that are dispersed in a continuous oil phase and stabilized by surfactant molecules at the water/oil interface. The surfactant-stabilized water pools provide a microenvironment for the preparation of nanoparticles by exchanging their contents via a fusio-redispersion process and preventing the excess aggregation of particles. As a result, the particles obtained in such a medium are generally very fine and monodisperse.

The objective of this work is the synthesis and the characterization of bimetallic Co@Ag nanoparticles with a core–shell structure. The microemulsion method has been selected as the synthesis method due to the control of the size of both the Co cores and the Ag shells as well as the simplicity of this method. TEM, XRD, XPS, UV–Vis, and electrochemical techniques have been used to characterize the obtained nanoparticles.

Experimental section

Synthesis procedure

Co_{core}–Ag_{shell} nanoparticles were prepared by the microemulsion method in a two-step reduction process at room temperature (25 °C). Water-in-oil microemulsions of water/polyethylenglycol-dodecylether (BRIJ®30)/*n*-heptane were used as microreactors where the reduction took place (Solla-Gullón et al. 2003). The size of the microemulsion droplet was determined by the molar ratio of water to surfactant (ω_0). In order to have micelles with the same size the molar ratio water to surfactant was maintained constant ($\omega_0 = 3.8$). The concentration of surfactant, in volume, amounted to 16.5% of the total microemulsion volume. For the preparation of the core–shell nanoparticles a two steps procedure was applied. The first step in which the cobalt core formation was carried out, equal volumes of two micellar solutions containing $Co(ClO_4)_2$ and the reductant, respectively, were mixed. After the mixing of the solutions, a clear change from pink to yellow was observed, indicating that the reduction process was taking place. The reaction (nucleation) took place essentially at the same time in the whole microemulsion media, which favored the formation of a large number of nuclei inside the water pools of the micelles. These nuclei grew very rapidly because of the material exchange between micelles. In a second step, identical volumes of two micellar solutions containing $AgClO_4$ and reducing agent, respectively, were poured over the microemulsion containing the cobalt cores. In this step, a change from yellow to dark brown was detected. After complete reduction, that took place in a few minutes, acetone was added to the solution to cause phase separation (Scheme 1 shows the procedure). The synthesized metallic nanoparticles were exhaustively washed with acetone in order to remove the surfactant. Among the advantages of this technique it is important to highlight not only the simplicity to prepare the nanoparticles with uniform size and composition, but also the capability to clean the surface of the nanoparticles.

Non-coated cobalt and silver nanoparticles were also prepared for comparison purposes. The methodology applied in their synthesis only implied one step of the process previously described: two microemulsions, one containing the metal salt ($Co(ClO_4)_2$ or $AgClO_4$) and the other one the reducing agent, were mixed and the particles were formed inside the droplets. After that, the nanoparticles were released from the microemulsion by adding acetone.

Chemicals and characterization methods

All chemicals used in this work, $AgClO_4$, $Co(ClO_4)_2$, $NaBH_4$ (borohydride), and N_2H_4 (hydrazine) were of analytical grade. Aqueous solutions were prepared with double distilled water treated then with a Millipore Milli Q system.

Transmission electron microscopy (TEM) and high-resolution TEM (HRTEM) experiments were performed with a JEOL 2100 microscope working at 200 kV. A drop of the nanoparticle dispersion was cast onto a carbon-coated copper grid sample holder followed by evaporation at room temperature. The compositional analysis of the nanoparticles was made by energy dispersive X-ray spectroscopy (EDS) coupled to TEM microscope.

X-ray diffractograms of the particles were recorded in a Siemens D-500 powder diffraction diffractometer. The Cu Kα radiation ($\lambda = 1.5418$ Å) was

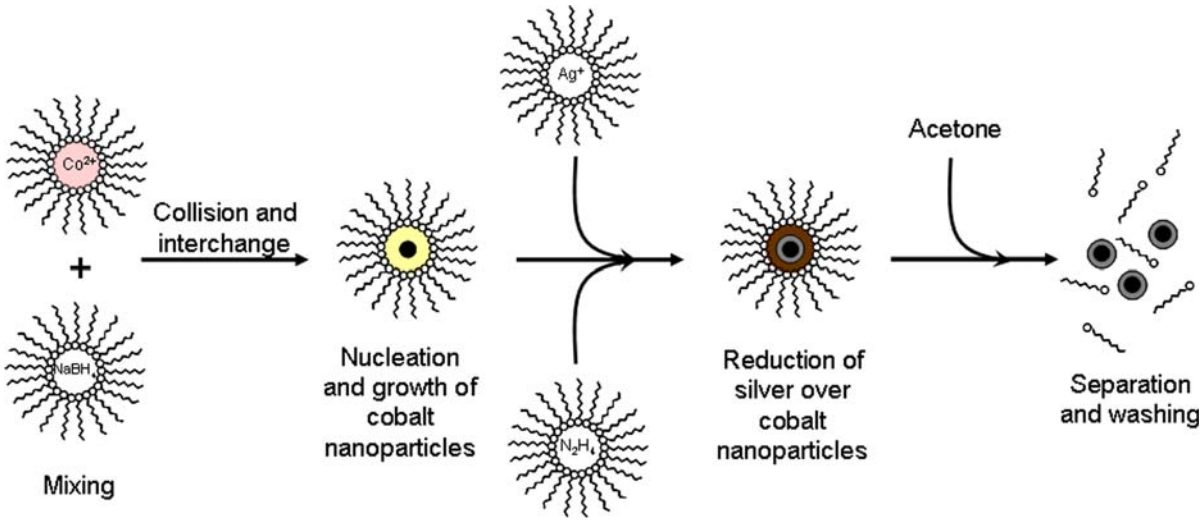

Scheme 1 Schematic illustration of the procedure for the synthesis of Co_{core}–Ag_{shell} nanoparticles [Co core (*black circle*), Ag shell (*gray circle*), and micelle (*white circles* plus *zigzag lines*)]

selected. X-ray powder diffraction diagrams were obtained in the 5–110 °2θ range with a step range of 0.05° and a measuring time of 15 s per step. Particles were placed over an oriented monocrystalline silicon substrate of low response for the measurements.

The UV–Vis spectra of w/o microemulsions containing nanoparticles were measured with a Shimadzu UV-1700 spectrophotometer using a 10-mm quartz cell.

X-ray photoelectron spectroscopy (XPS) measurements were performed with a PHI 5600 multitechnique system and Auger spectroscopy measurements were done with a PHI 670 scanning Auger nanoprobe system. The binding energies (BE) of the XPS signals of all species have been corrected by assuming C1s signal at 284.6 eV

Electrochemical experiments were performed in a conventional three electrode cell using a potentiostat/galvanostat Autolab PGSTAT12. Before measurements, solutions were deaerated by bubbling argon and maintained under argon atmosphere during the experiments. Cyclic voltammograms were made at 25 °C. A spiral platinum wire was used as the counter electrode and Ag/AgCl/3 M NaCl/0.1 M $NaClO_4$ as the reference one. The working electrode was a vitreous carbon rod of 2 mm of diameter.

Results and discussion

Optimization of preparation conditions

The first attempt in the Co@Ag synthesis optimization was to find out the minimum stable cobalt core size. At least a 0.067 M $Co(ClO_4)_2$ solution was necessary, as smaller concentrations led to unstable nucleus and hence no nanoparticles were formed. A strong reducing agent ($NaBH_4$) was needed due to the low reduction capacity of cobalt. In this sense, a 1:15 cobalt(II):sodium borohydride ratio was demonstrated as the more adequate.

Due to the ease silver reduction, a milder reducing agent than borohydride was required during the Co@Ag synthesis. Hydrazine was selected as it allows controlling feasibly the monodispersity of the particle size because the reduction takes place in a slower way. A 1:10 silver(I):hydrazine ratio was demonstrated as the optimum ratio.

During the synthesis all the microemulsions were stirred by means of ultrasounds in a sonicating bath instead of shaking because of the obtained nanoparticles showed higher monodispersity.

In this study, different Co@Ag nanoparticles were prepared. The cobalt core was fixed as the minimum one achieved. On the other hand, different $AgClO_4$

concentrations in the micellar solution were used in order to obtain variable Ag-shell thicknesses. The Co:Ag molar ratio of the nanoparticles prepared were in the range 1:1–1:2.5.

In some conditions, reduction with sodium borohydride can give rise to the formation of borides (Schlesinger et al. 1953). However, in microemulsions with low water to surfactant ratios (conditions used in this work) water is mainly linked and highly immobilized by the surfactant heads and hence no cobalt–boron compounds are expected (Garcia-Bastida et al. 2005).

Morphology and structure

Transmission electron microscopy was used to evaluate the particle shape and size. Figure 1 shows some micrographs of the obtained Co@Ag nanoparticles. It can be seen that the particles are quasi-spherical in shape with highly uniform size and relatively dispersed. However, some aggregates were observed on the TEM grids probably due to the nanoparticle's aggregation after drying on the copper grid. Analysis of this and several other images reveals that the particles have a mean size of 3 nm for Co:Ag ratio 1:1.5 and 5 nm for Co:Ag ratio 1:2.5. The nanoparticles with Co:Ag molar ratios higher than 1:1.5 show incomplete silver coverage.

On the other hand, in order to demonstrate the bimetallic nature of the particles the micrographs were highly underfocused with the idea to enhance the nanoparticle TEM contrast as Crisan et al. have shown (Crisan et al. 2006). This procedure reveals a dark core and a shiny shell (insets Fig. 1a, d) giving a first clue about the core–shell nature of the synthesized nanoparticles.

The Selected Area Electron Diffraction (SAED) patterns recorded from the different $Co_{core}Ag_{shell}$ nanoparticles are shown in Fig. 1c, f. The patterns are a complex ring pattern, characteristic for polycrystalline materials, which comprises two different crystal structures. The *d* values calculated from the positions of the electron diffraction rings agreed well with the *d* values reported for (111), (200), (220), and (311) planes of fcc silver and the (100), (002), and (101) planes of hcp cobalt. Moreover, no evidence of fcc cobalt was found. The presence of cobalt oxides cannot be discarded. In this sense, other techniques will be used to confirm or not the presence of these species.

Although a correct core–shell formation has been observed by TEM studies, in order to univocally assure the formation of this structure, HRTEM was required to have a deeper insight of the detailed structure and the nature of the crystalline symmetry for the Co and Ag phases in the bimetallic nanoparticles. HRTEM investigations of single particles revealed a multiple twinned or polycrystalline nature of the nanoparticles. Interplanar spacings could be directly determined from the images by measuring the lattice fringes (Fig. 2a). On the other hand, Fast Fourier Transformation (FFT) was also performed on the HRTEM images of single particles (Fig. 2b). The interplanar spacing 2.351 Å (spots 1, 2) corresponding to fcc-Ag (111) was detected in the nanoparticles shell (upper left FFT pattern of Fig. 2b). On the other

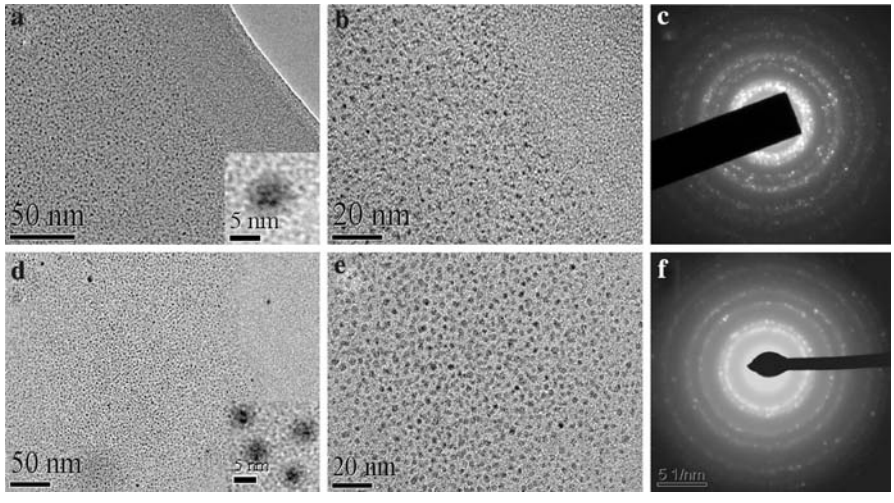

Fig. 1 **a–c** TEM micrographs and SAED pattern of Co:Ag ratio 1:1.5 nanoparticles. **d–f** TEM micrographs and SAED pattern of Co:Ag ratio 1:2.5 nanoparticles

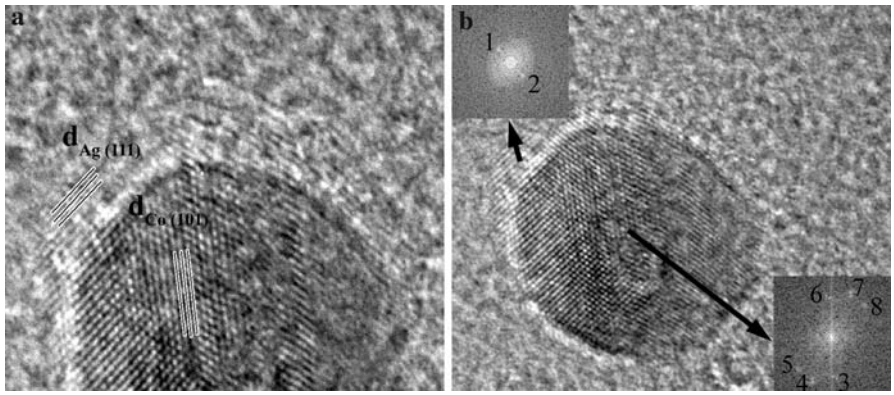

Fig. 2 HRTEM micrographs of a Co:Ag ratio 1:1.5 nanoparticle. **a** Determination of the interplanar spacings by measuring the lattice fringes directly from the image. **b** Determination of the interplanar spacings by FFT

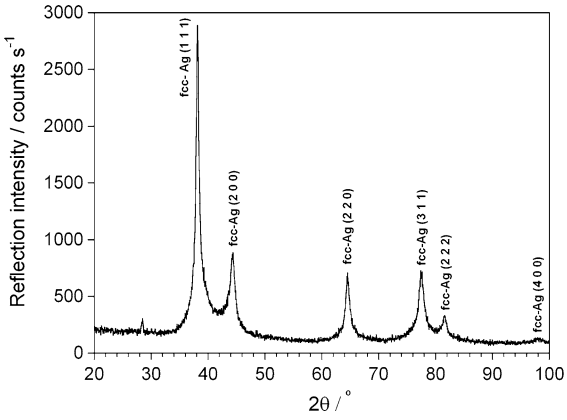

Fig. 3 X-ray diffraction pattern for Co:Ag ratio 1:1.5 nanoparticles

hand, *d* spacings of 2.348, 2.175, and 1.925 Å attributed to fcc-Ag (111) (spots 3, 6), hcp-Co (100) (spots 5, 8) and hcp-Co (101) (spots 4, 7), respectively, were detected when the FFT analysis was performed in the nanoparticle's center (including both the core and the shell) (lower right FFT pattern of Fig. 2b). Both procedures allowed us to determine interplanar spacings corresponding to fcc silver and hcp cobalt, results in agreement with those found by means of SAED measurements. From this study, one can conclude that cobalt is mainly localized in the central area meanwhile silver occupies the edges of the nanoparticle, thus obtaining a core–shell structure.

Figure 3 shows a typical XRD pattern of the as-prepared Co@Ag samples. A well-defined pattern can be clearly seen. Peaks corresponding to the presence of fcc silver can only be detected. However, peaks or bands corresponding neither metallic cobalt nor cobalt oxides are observed. These results agree with those reported by A. J. Garcia-Bastida et al. in the sense that no Bragg reflections for cobalt were detected (Garcia-Bastida et al. 2005). Meanwhile, other works dealing with nanoparticles of higher size reported the presence of both Co and Ag reflections (Bala et al. 2004). The dissimilar particle sizes could explain the observed results. On the other hand, the fact not to observe the Bragg reflections of the metal core by XRD could be indicative of a correct core–shell formation (Iglesias-Silva et al. 2007; Mandal et al. 2005).

Figure 4a shows a TEM image of non-coated cobalt nanoparticles. Very small nanoparticles, with sizes smaller than 1 nm, are observed. Because of the very small size of the nanoparticles the precise estimation of the size is very difficult. The XRD pattern shown in Fig. 4b reveals the presence of six bands, located at 20.6°, 34.0°, 43.4°, 46.8°, 59.5°, and 82.3°. The Bragg reflections of the XRD pattern are difficult to be univocally assigned to metallic cobalt or some cobalt oxides because of the overlapping of the different bands. In this sense, XPS of the non-coated cobalt nanoparticles will be performed in order to reveal the nature of cobalt. Moreover, the fact to observe bands instead of peaks is in agreement with the small size of the nanoparticles detected by TEM.

XPS characterization

XPS technique was carried out in order to have a more accurate knowledge about the oxidation states of cobalt in the synthesized nanoparticles. Figure 5a shows the XPS spectra of the Co:Ag ratio 1:1.5 nanoparticles. The surface chemical composition

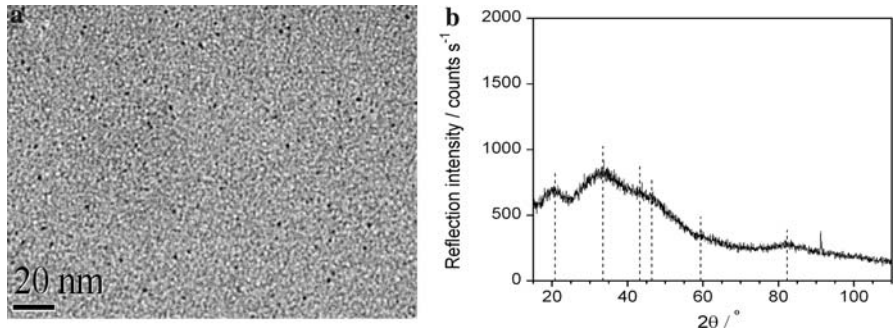

Fig. 4 **a** TEM micrograph and **b** XRD pattern of non-coated Co nanoparticles

revealed the presence of the elements O, C, Co, and Ag. Moreover, no boron was detected in the recorded spectra (BE(B 1s) = 190 eV) corroborating that the synthesis conditions employed avoid the formation of Co–B compounds. On the other hand, the fact to observe Co is because the penetration depth of the XPS beam used is around 2 nm, penetration depth higher than the thickness of the silver shell. The O 1s spectrum (Fig. 5b) was composed of two peaks at 530.4 and 531.7 eV attributed to cobalt oxides and surface contamination, respectively. As it can be observed in the Ag 3d spectrum of Fig. 5c, the peak $3d_{5/2}$ was centered at a BE 366.2 eV; meanwhile $3d_{3/2}$ was placed at a BE 372.2 eV. These values are lower than those reported for bulk metallic silver (BE(Ag $3d_{5/2}$) = 368.1, BE(Ag $3d_{3/2}$) = 374) (Galuri et al. 1999). Although the BE for the oxides (BE(AgO $3d_{5/2}$) = 367.3 and BE(Ag_2O $3d_{5/2}$) = 367.7) (Hoflund et al. 1994a, b) fits better than metallic silver the existence of silver oxides is discarded. On one hand, the calculated full width half maximum (FWHM) of 1.1 eV agrees with the peak width for metallic silver (1.2 eV) (Galuri et al. 1999) as the values for the different oxides are higher than 1.50 eV (Hoflund et al. 1994a, b). The energy separation between $3d_{5/2}$ and Ag $3d_{3/2}$ (ΔBE = 6.0 eV) also agrees with that tabulated (Chastain 1992). On the other hand, the O 1s BE corresponding to the different silver oxides are 528.5 eV (AgO) and 528.8 eV (Ag_2O) (Hoflund et al. 1994a, b), values which do not fit with the BE for the O 1s peaks reported here. Moreover, XRD discard the presence of silver oxides. The authors attribute this shift in the Ag 3d photopeak's BE to the different chemical environment respect pure silver, the cobalt core could modify the energy levels and hence a different BE could be obtained. Similar results have been previously found for silver nanoparticles on silica spheres (Luo et al. 2009). The Co 2p spectrum shows a complex profile (Fig. 5d). Two states that contribute to the main Co $2p_{3/2}$ feature can be identified at BE of 778.1 and 779.3 eV, compatible with metallic cobalt and various oxides (CoO or Co_3O_4), respectively. Moreover, the Co $2p_{1/2}$ shows two main peaks located at 793.4 and 795.5 eV, in which the peak placed at BE = 793.4 eV fits well with that tabulated for metallic cobalt; meanwhile, the peak at BE = 795.5 eV agrees with Co(II) in the form of CoO. Close to the main peaks two intense satellites located at the high binding-energy side of the main photopeaks are present, which are characteristic of the CoO spectra (Jiménez et al. 1998; Chuang et al. 1976).

Similar features of the XP spectrum for Co:Ag ratio 1:2.5 were observed except for the fact that a very weak cobalt signal was detected (Fig. 5e, h) indicating that the XP beam scarcely penetrates until the cobalt core because of the thicker silver shell. For oxygen (Fig. 5f) only the peak related to surface contamination was observed. Meanwhile, the O 1s peak previously attributed to cobalt oxides and placed at BE 530.4 eV did not appear as the beam hardly penetrate until the cobalt core. However, the presence of CoO in the nanoparticles is also expected. The recorded spectrum of Ag 3d (Fig. 5g) shows almost the same features as those previously described. The difference is that the 3d photopeaks appear at BE closer to the values of metallic silver. The higher the silver quantity, the lesser the influence of the chemical environment (the cobalt core) and hence the behavior start to approach that of pure silver.

The XP spectrum of non-coated cobalt nanoparticles showed the unique presence of C, O, and Co. The O 1s spectrum shows the two peaks related to cobalt oxides and surface contamination. On the other hand,

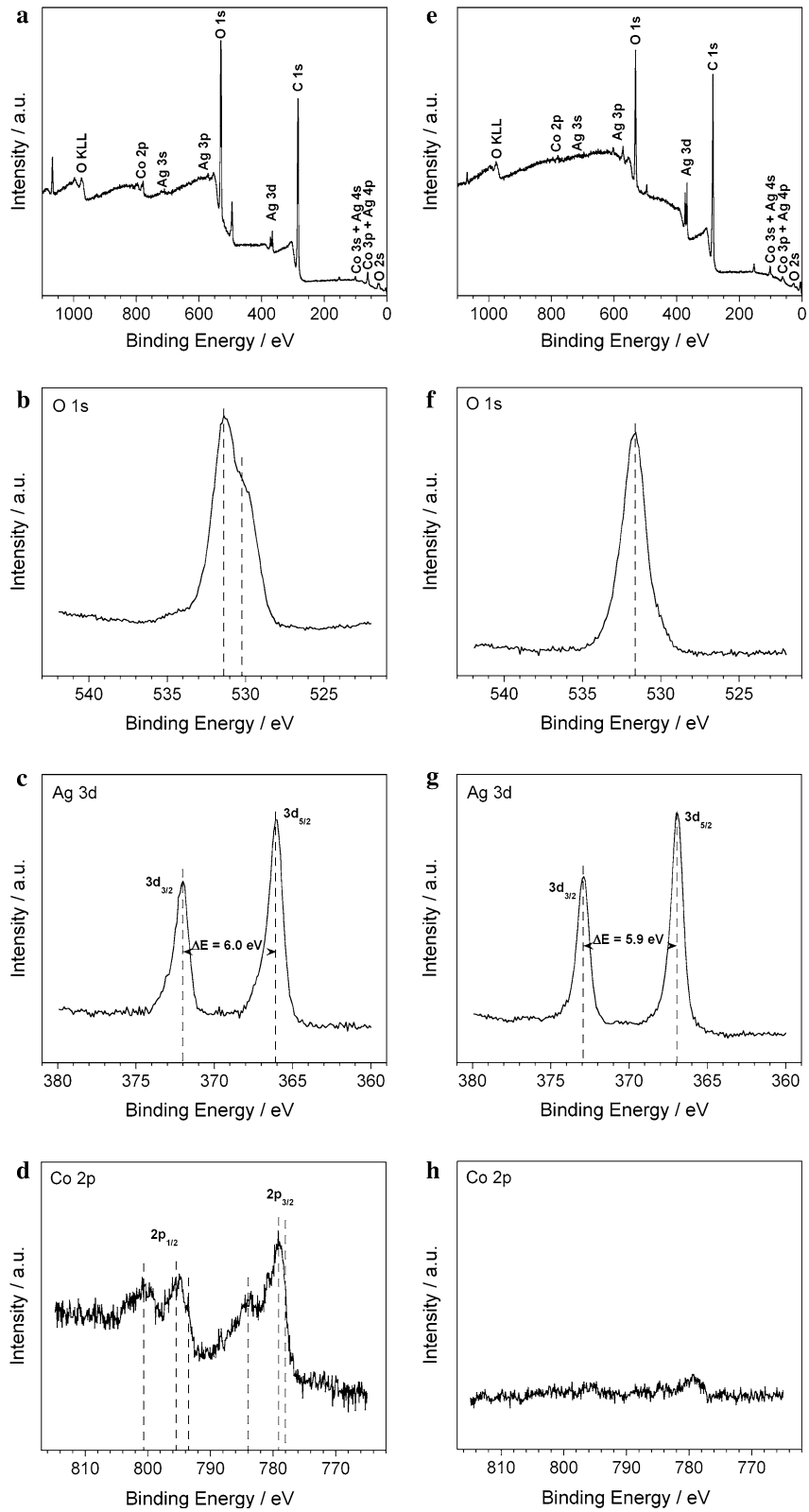

Fig. 5 XPS spectrum and O 1s, Co 2p, and Ag 3d spectra of **a–d** Co:Ag molar ratio 1:1.5 nanoparticles and **e–h** Co:Ag molar ratio 1:2.5 nanoparticles

the Co 2p spectrum resembles that of the Fig. 5d. The only difference to note here is that the peaks related to metallic cobalt are weaker than in the Co@Ag nanoparticles because of the absence of the silver protective layer.

Optical properties

The optical properties of the Co@Ag nanoparticles have been studied by UV–Visible spectroscopy. Figure 6 shows the UV–Vis adsorption spectrum of the Co@Ag colloid dispersion as well as the spectra of pure Ag and Co colloid dispersions for comparison purposes. The UV–Vis spectrum of Co nanoparticles is almost featureless along the whole scanned wavelength range except for a monotonic absorbance increase at the shorter wavelengths and a very small band located around 350 nm (Fig. 6, dotted line). This absorption can be ascribed to the presence of cobalt oxides (Ershov et al. 2000). On the other hand, the silver colloids exhibit one absorption band with a maximum centered at 404 nm (Fig. 6, continuous line) characteristic of the optical properties of Ag nanostructures. Meanwhile, the absorption spectrum of the Co@Ag colloids (Fig. 6, dashed line) shows a slight red-shift in the surface plasmon (SP) resonance peak (418 nm) and an increase in the bandwidth respect to that recorded from pure-Ag colloids. The observed shift in the SP peak has been previously reported for gold-coated iron oxide (Lyon et al. 2004)

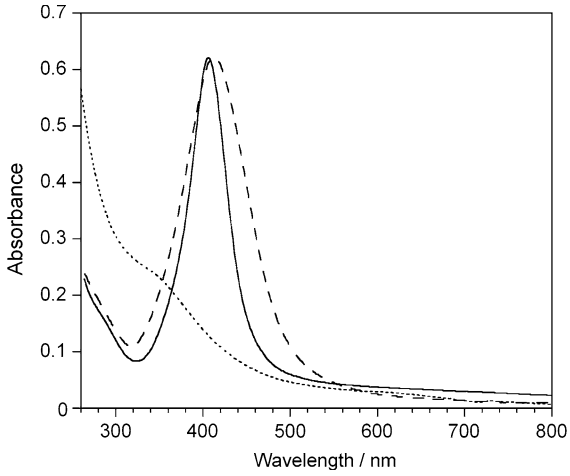

Fig. 6 UV–Vis spectra for *dotted line*—cobalt micellar solution, *continuous line*—silver micellar solution, and *dashed line*—$Co_{core}Ag_{shell}$ micellar solution

and silver-coated nickel nanoparticles (Gaudry et al. 2001), this finding suggesting that a significant amount of pure silver nanoparticles in the samples is unlikely. It is worthy to remark again that the absorption spectrum of Co@Ag nanoparticles is broader than that of pure Ag. The phenomenon was similar to that obtained by the extended Mie theory for a Ni_{core}–Ag_{shell} nanoparticle and it was attributed to the fact that Ag was covered on the surface of the Ni cores (Gaudry et al. 2001; Portales et al. 2002; Jackson and Halas 2001) corroborating the core–shell nature of the synthesized Co–Ag nanoparticles.

Electrochemical behavior

Electrochemical characterization of the prepared nanoparticles was carried out in a 0.1 M $NaClO_4$ solution by means of cyclic voltammetry. The experiments were carried out at a scan rate of 10 mV s^{-1} using vitreous carbon rod of 2 mm of diameter as a working electrode. The voltammetric response of the substrate reveals that no current related to electrode oxidation/reduction processes were recorded between the potentials associated to the initio of hydrogen and oxygen evolution (see inset Fig. 7a). No differences were observed independently of the direction scan.

A drop of the nanoparticles dispersion was deposited by gravity over the vitreous carbon substrate. A nitrogen atmosphere was used to evaporate the solvent. This evaporation procedure gives a good contact between the substrate and the nanoparticles. Before each experiment the substrate was mechanically polished with alumina and rinsed with ultrapure water to remove the nanoparticles from previous experiments.

The cyclic voltammetry of freshly Co@Ag nanoparticles was recorded scanning at first toward positive potentials from a potential where no initial current was recorded. A clear oxidation peak (A) followed by a band (B) prior to oxygen evolution was observed. Reversing the scan, reduction current (C) was detected around 0 mV (Fig. 7a, dashed line). The negative current feature did not appear when the solution was stirred during the negative sweep. No more remarkable features were observed in the negative scan previous to hydrogen evolution.

Similar experiments were performed depositing either silver (Fig. 7a, continuous line) or non-coated

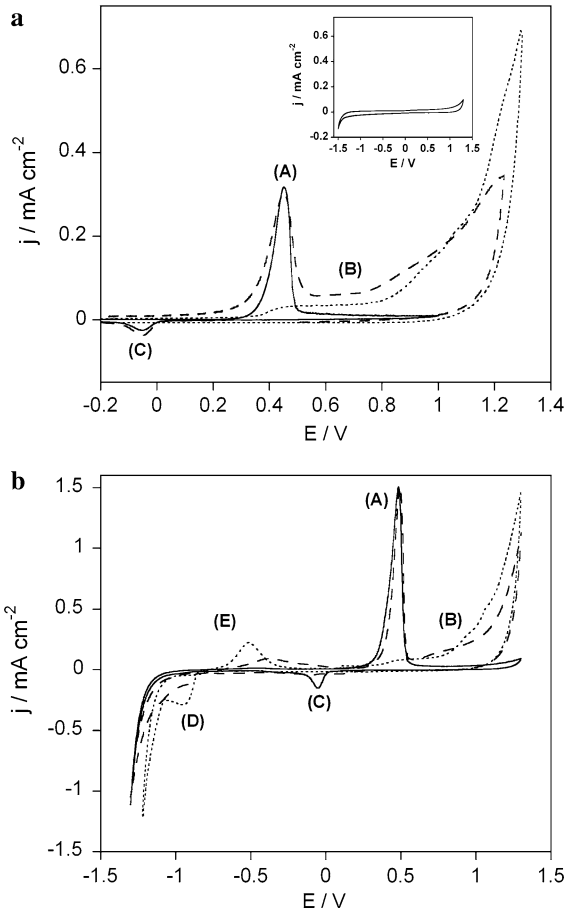

Fig. 7 **a** Cyclic voltammograms for *dashed line*—Co@Ag, *continuous line*—silver, and *pointed line*—cobalt nanoparticles. Scanning from −0.5 V toward positive potentials. The inset shows the voltammetric response of the vitreous carbon (working electrode). **b** Cyclic voltammograms for *dashed line*—cobalt nanoparticles, *pointed line*—Co:Ag molar ratio 1:1 nanoparticles (which are not completely cover), and *continuous line*—Co:Ag molar ratio 1:1.5 nanoparticles (which are completely cover). Scanning from −0.5 V toward negative potentials

cobalt nanoparticles (Fig. 7a, dotted line). The voltammetric results obtained from the single metal nanoparticles allowed us to identify the features observed in the Co@Ag voltammograms. The peak (A) and the band (B) recorded during the positive scan are related to silver and cobalt oxidation, respectively. The observed current (C) appears in the voltammograms of Ag and Co@Ag nanoparticles during the negative scan and recorded under quiescent conditions, whereas it does not appear when stirring. This current was related to the reduction of the oxidized silver species that remained near the electrode when the experiments were made under quiescent conditions.

Another series of experiments were performed scanning at first toward negative potentials. The non-coated cobalt nanoparticles showed a current plateau (D) previous to hydrogen evolution (Fig. 7b, dotted line). However, this plateau was not recorded in the silver nanoparticles voltammogram. Other remarkable feature is that the beginning of hydrogen evolution took place at more positive potentials over cobalt nanoparticles than over silver nanoparticles, as expected, because of the catalytic properties of cobalt. During the positive scan a symmetric band (E) centered at −450 mV and a band at positive potentials (B) appeared in the non-coated cobalt nanoparticles voltammogram; meanwhile no features were recorded in the silver voltammograms before the sharp oxidation peak (A). The symmetric band (E) is related to the plateau (D) recorded previous to hydrogen evolution.

Taking profit of the characteristic voltammetric response observed for both Co and Ag nanoparticles when the scan was followed toward the negative direction, different Co–Ag nanoparticles (previously characterized by TEM) were analyzed by cyclic voltammetry scanning at first toward negative potentials. The results indicate that for those particles in which TEM studies revealed an incomplete silver coverage of the nuclei, some cobalt-related reduction current (D) before hydrogen evolution was recorded (Fig. 7b, dashed line). It was also observed that the worst the Ag shell is the higher the cobalt-related current is. However, no cobalt-related current was observed in those particles with a perfect core–shell structure neither on the negative-going scan nor on the positive-going sweep (Fig. 7b, continuous line). Moreover, the appearance of hydrogen evolution over Co@Ag nanoparticles not completely coated took place between the hydrogen evolution potentials observed over silver and cobalt nanoparticles. However, for those Co@Ag nanoparticles completely covered the evolution of hydrogen begun at similar potentials than over silver nanoparticles.

The cobalt-related negative current (D) might be related to the reduction of cobalt oxides that were formed over cobalt surface after its deposition. After cobalt oxides reduction, hydrogen was adsorbed over cobalt and remained attached to the metal until being

oxidized during the positive scan leading to the symmetric band (E).

These results prove that voltammetric experiments may be used as a qualitative tool to check the goodness of the prepared Co@Ag nanoparticles. This simple procedure will allowed to determine the correct core–shell formation. In this sense, cyclic voltammetry would be a cheap and feasible alternative to TEM studies during the optimization of the Co@Ag preparation conditions to establish the formation of a true Co_{core}–Ag_{shell} particle. Evidently, the TEM is an irreplaceable tool for measuring the particles shape and size as well as to corroborate the findings obtained by means of other complementary techniques.

Conclusions

An easy method for the synthesis of Co@Ag nanoparticles based on successive reactions in microemulsions has been used. This method has been revealed as a feasible one to prepare core–shell nanoparticles. The particle size analysis indicated that all the synthesized bimetallic nanoparticles were highly monodisperse and presented a mean size that fell in the range 3–5 nm, depending on the preparation concentrations. HRTEM joined to SAED and FFT allowed to determine the crystalline structure of both Ag (fcc) and Co (hcp). Moreover, it was possible to conclude that cobalt was mainly localized in the central area meanwhile silver occupied the edges of the nanoparticle, thus obtaining a core–shell structure. Moreover, the other techniques employed corroborated the synthesis of Co_{core}–Ag_{shell} nanoparticles. On one hand, XRD showed the unique presence of the fcc-Ag phase (no cobalt reflections were detected) fact that could be indicative of a correct core–shell formation. On the other hand, UV–Vis of Co@Ag nanoparticles showed a red-shift in the SP resonance peak as well as an increase in the bandwidth respect to that recorded from silver colloids, both findings suggesting again the core–shell nature of the synthesized Co@Ag nanoparticles. XPS analysis allowed us to identify the presence of metallic cobalt and cobalt oxides in the nuclei. Moreover, no appreciable Co 2p signal was recorded upon increasing the silver shell thickness as the XP beam scarcely penetrates until the cobalt core. Finally, cyclic voltammetry experiments allowed us to determine the correct core–shell formation taking advantage of the different electrochemical behavior of cobalt, silver, and Co@Ag nanoparticles when the scan was toward negative direction.

Acknowledgments The authors are grateful to Dr. J. Solla-Gullón for their helpful support in the preparation of the nanoparticles. This article was supported by contract MAT-2006-12913-C02-01 from the *Comisión Interministerial de Ciencia y Tecnología* (*CICYT*). J. García-Torres would also like to thank the Departament d'Innovació, Universitats i Empresa of the Generalitat de Catalunya and Fons Social Europeu for their financial support.

References

Andres RP, Bein T, Dorogi M, Feng S, Henderson JI, Kubiak CP, Mahoney W, Osifchin RG, Reifenberger R (1996) "Coulomb staircase" at room temperature in a self-assembled molecular nanostructure. Science 272:1323–1325

Bala T, Arumugam SK, Pasricha R, Prasad BLV, Sastry M (2004) Foam-based synthesis of cobalt nanoparticles and their subsequent conversion to $Co_{core}Ag_{shell}$ nanoparticles by a simple transmetallation reaction. J Mater Chem 14:1057–1061

Chastain J (1992) Handbook of X-ray photoelectron spectroscopy. Perkin-Elmer Coorp, MN

Chuang TJ, Brundle CR, Rice DW (1976) Interpretation of the x-ray photoemission spectra of cobalt oxides and cobalt oxide surfaces. Surf Sci 59:413–429

Crisan O, Angelakeris M, Simeonidis K, Kehagias T, Komninou P, Giersig M, Flevaris NK (2006) Structure effects on the magnetism of AgCo nanoparticles. Acta Mater 54:5251–5260

Ershov BG, Sukhov NL, Janata E (2000) Formation, absorption, spectrum, and chemical reactions of nanosized colloidal cobalt in aqueous solution. J Phys Chem B 104:6138–6142

Galuri E, Güldur C, Srivsnnavit S, Osuwan S (1999) CO oxidation by silver cobalt composite oxide. Appl Catal A Gen 182:147–163

Garcia-Bastida AJ, Rivas J, Lopez-Quintela MA, Gonzalez-Penedo A, Traverse A (2005) Synthesis and structural characterization of Co immersed in Ag nanoparticles obtained by successive reactions in microemulsions. Sci Technol Adv Mat 6:411–419

Gaudry M, Lermé J, Cottancin E, Pellarin M, Prével B, Treilleux M, Mélinon P, Rousset JL, Broyer M (2001) Size and concentration effects in the optical properties of alloyed $(Au_xAg_{1-x})_n$ and core-shell $(Ni_xAg_{1-x})_n$ embedded clusters. Eur Phys J D 16:201–204

Halperin WP (1986) Quantum size effects in metal particles. Rev Mod Phys 58:533–606

Hodak JH, Henglein A, Hartland GV (2000) Coherent excitation of acoustic breathing modes in bimetallic core–shell nanoparticles. J Phys Chem B 104:5053–5055

Hoflund GB, Weaver JF, Epling WS (1994a) AgO XPS spectra. Surf Sci Spectra 3(2):163–168

Hoflund GB, Weaver JF, Epling WS (1994b) Ag_2O XPS spectra. Surf Sci Spectra 3(2):157–162

Hyeon T, Lee SS, Park J, Chung Y, Na HB (2001) Synthesis of highly crystalline and monodisperse maghemite nanocrystallites without a size-selection process. J Am Chem Soc 123:12798–12801

Iglesias-Silva E, Rivas J, León Isidro LM, López-Quintela MA (2007) Synthesis of silver-coated magnetite nanoparticles. J Non-Cryst Solids 353:829–831

Jackson JB, Halas NJ (2001) Silver nanoshells: variations in morphologies and optical properties. J Phys Chem B 105:2743–2746

Jiménez VM, Espinós JP, González-Elipe AR (1998) Control of the stoichiometry in the deposition of cobalt oxides on SiO_2. Surf Interface Anal 26:62–71

Luo N, Mao L, Jiang L, Zhan J, Wu Z, Wu D (2009) Directly ultraviolet photochemical deposition of silver nanoparticles on silica spheres: preparation and characterization. Mater Lett 63:154–156

Lyon JL, Fleming DA, Stone MB, Schiffer P, Williams ME (2004) Synthesis of Fe oxide core/Au shell nanoparticles by iterative hydroxylamine seeding. Nano Lett 4:719–723

Mandal M, Kundu S, Ghosh SK, Panigrahi S, Sau TK, Yusuf SM, Pal T (2005) Magnetite nanoparticles with tunable gold or silver shell. J Colloid Interface Sci 286:187–194

Portales H, Saviot L, Duval E, Gaudry M, Cottancin E, Pellarin M, Lermé J, Broyer M (2002) Resonant Raman scattering by quadrupolar vibrations of Ni–Ag core–shell nanoparticles. Phys Rev B 65:165422

Schlesinger HI, Brown HC, Finholt AE, Gilbreath JR, Hoekstra HR, Hyde EK (1953) Sodium borohydride, its hydrolysis and its use as a reducing agent and in the generation of hydrogen. J Am Chem Soc 75:215–219

Schmid G (1994) Clusters and colloids, from theory to applications. VCH, Weinheim

Schmid G (1998) Metal clusters and colloids. Adv Mater 10:515–526

Solla-Gullón J, Montiel V, Aldaz A, Clavilier J (2003) Synthesis and electrochemical decontamination of platinum–palladium nanoparticles prepared by water-in-oil microemulsion. J Electrochem Soc 150(2):E104–E109

Tourinho FA, Franck R, Massart R (1990) Aqueous ferrofluids based on manganese and cobalt ferrites. J Mater Sci 25:3249–3254

7.2. Magnetic and magnetotransport properties

The magnetic properties of the $Co_{Core}Ag_{Shell}$ nanoparticles were also measured. Figure 7.1 shows the magnetization-magnetic field curve in which no hysteresis and a high magnetic field at which saturation magnetization is reached (around 20 kOe) are observed. Both results indicate the superparamagnetic behaviour of the synthesized nanoparticles which is also in agreement with the small size of the cobalt core. On the other hand, a saturation magnetization value of around 53 emu g^{-1} was obtained, it being smaller than that corresponding to pure cobalt. The observed decrease in magnetization could be attributed to partial surface oxidation.

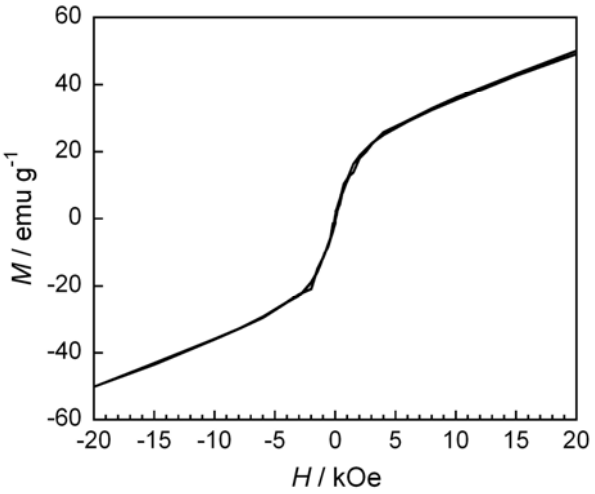

Figure 7.1. Magnetic hysteresis loop of the synthesized $Co_{Core}Ag_{Shell}$ nanoparticles.

The magnetotransport properties of the $Co_{Core}Ag_{Shell}$ were also investigated. However, the measurement of the magnetoresistance was a challenge due to technical difficulty to perform electrical contacts on the nanoparticles. The only study dealing with the magnetoresistance of nanoparticle made the measurement in compressed thick pellets [71]. It was confirmed that the nanoparticles were completely destroyed by the compression and therefore, this method was discarded. In this sense, a strategy was developed to perform the magnetoresistance measurements. The steps followed to make the electrical contacts are schematized in figure 7.2A. A non-conductive glass substrate was selected to deposit the nanoparticles in order to force the electrical current to pass trough the metallic nanoparticles. Firstly, four gold stripes of 200 μm wide were sputtered over the glass substrate employing a mask. After that, nanoparticles were placed over the glass with the sputtered gold stripes by surface tension. A high amount of nanoparticles were deposited in order to favour the electrical contact among them.

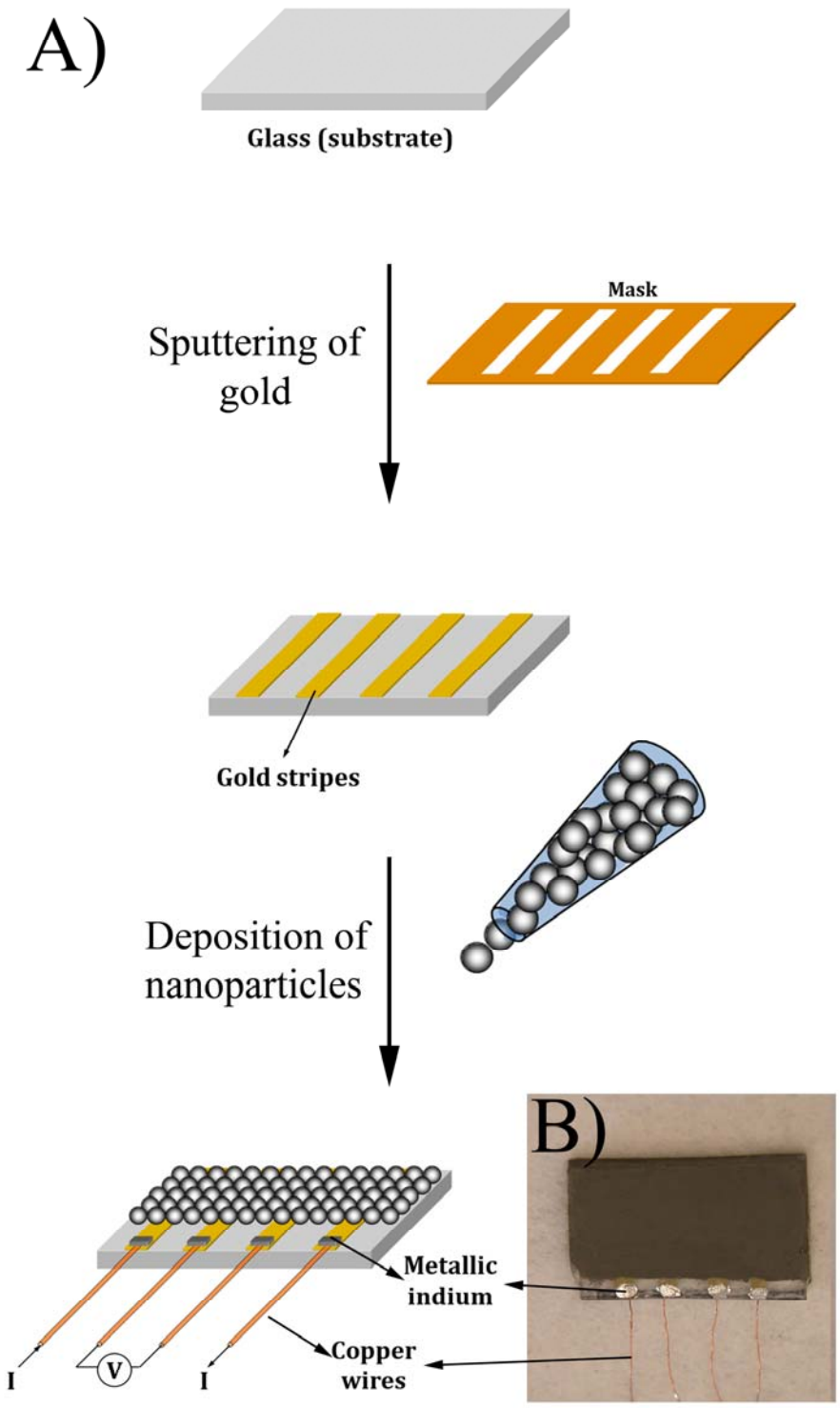

Figure 7.2. Steps followed to perform the magnetoresistance measurement in nanoparticles.

Finally, copper wires were attached to the gold stripes using small amounts of metallic indium. The result is shown in figure 7.2B in which it can be observed that nanoparticles completely cover the four gold stripes. Moreover, electrical contact exists between the different stripes indicative of the conductive behaviour of the nanoparticles.

The method was revealed successful to measure the magnetoresistance of nanoparticles (Figure 7.3). The magnetoresistance curves were characterized by no saturation of the magnetoresistance even at the highest applied magnetic field and no splitting around 0 kOe, both factors being indicative of the unique presence of superparamagnetic particles. Small GMR values were recorded for the fabricated nanoparticles, the maximum value being 0.1 % at room temperature. However, this value is higher than that reported for Co-Ag nanoparticles for which GMR was only detected at 2 K [71].

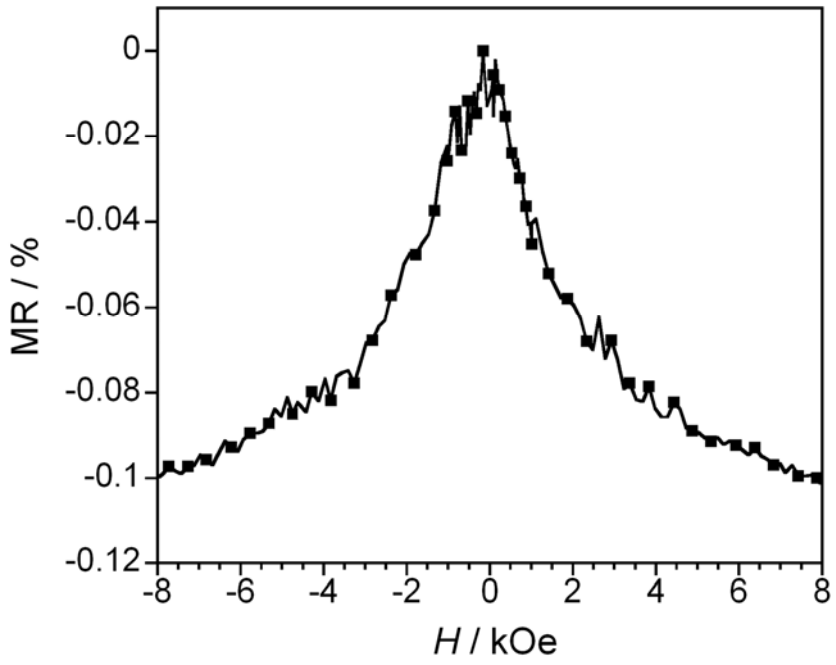

Figure 7.3. MR(H) curve of $Co_{Core}Ag_{Shell}$ nanoparticles measured applying the procedure previously described.

7.3. Summary and outlook

Co-Ag nanoparticles have been successfully prepared by an easy method as the microemulsion method is. Although all the characterization techniques employed were in agreement with a core-shell arrangement in which cobalt was in the nanoparticle inner whereas silver was in the outer, HRTEM studies were essential to confirm it. Moreover, the electrochemical technology has been successfully employed to discriminate the correct core-shell structure formation. Magnetic and magnetotransport properties corroborated the superparamagnetic behaviour of the nanoparticles as it was expected attending the small size detected by TEM. It was necessary to develop a strategy to proceed to the magnetoresistance measurement which was revealed successful for the measurement of nanoparticles. The synthesized $Co_{Core}Ag_{Shell}$ nanoparticles showed GMR values up to 0.1 %. Nanoparticles are very interesting for magnetotransport properties measurement not only because of the size of magnetic/non-magnetic nanoparticles can be easily modified but also the nearly monodisperse size that can be obtained. However, much more progress could be maid in this field since a great number of parameters can be modified, i.e. cobalt core size, silver shell thickness or influence of annealing, just to mention a few.